On ZRP wind input term consistency in Hasselmann equation

Vladimir Zakharov[1,2,3,4], Donald Resio[5], and Andrei Pushkarev[1,2,3,4]

[1]Department of Mathematics, University of Arizona, Tucson, AZ 85721, USA
[2]Lebedev Physical Institute RAS, Leninsky 53, Moscow 119991, Russia
[3]Novosibirsk State University, Novosibirsk, 630090, Russia
[4]Waves and Solitons LLC, 1719 W. Marlette Ave., Phoenix, AZ 85015, USA
[5]Taylor Engineering Research Institute, University of North Florida

Correspondence to: Andrei Pushkarev (dr.push@gmail.com)

Abstract.

The new ZRP wind input source term (Zakharov et al., 2012) is examined for its theoretical consistency via numerical simulation of Hasselmann equation. The results are compared to field experimental data, collected at different sites around the world, and theoretical predictions based on self-similarity analysis. Good agreement is obtained for both limited fetch and time domain statements.

1 Introduction

The scientific description of wind driven wave seas, inspired by solid state physics statistical ideas (see, for instance, Nordheim (1928)), was proposed by Hasselmann (1962, 1963) in the form of the kinetic equation for waves:

$$\frac{\partial \varepsilon}{\partial t} + \frac{\partial \omega_k}{\partial \boldsymbol{k}} \frac{\partial \varepsilon}{\partial \boldsymbol{r}} = S_{nl} + S_{in} + S_{diss} \tag{1}$$

where $\varepsilon = \varepsilon(\omega_k, \theta, \boldsymbol{r}, t)$ is the wave energy spectrum, as a function of wave dispersion $\omega_k = \omega(k)$, angle θ, two-dimensional real space coordinate $\boldsymbol{r} = (x, y)$ and time t. S_{nl}, S_{in} and S_{diss} are the nonlinear, wind input and wave-breaking dissipation source terms, respectively. Hereafter, only the deep water case, $\omega = \sqrt{gk}$ is considered, where g is the gravity acceleration and $k = |\boldsymbol{k}|$ is the absolute value of the vector wavenumber $\boldsymbol{k} = (k_x, k_y)$.

Since Hasselmann's work, Eq.(1) has become the basis of operational wave forecasting models such as WAM, SWAN and Wavewatch III (Tolman, 2013; SWAN). While the physical oceanography community consents on the general applicability of Eq.(1), there is no consensus agreement on universal parameterizations of the source terms S_{nl}, S_{in} and S_{diss}.

The S_{nl} term was derived by different methods from the Euler equations for free surface incompressible potential flow of a liquid by Hasselmann (1962, 1963) and Zakharov and Filonenko (1966). This term is a complex nonlinear operator acting on ε_k, concealing hidden symmetries (Zakharov and Filonenko, 1967; Zakharov et al., 1992). Resio and Perrie (1991) showed that those different forms are identical on the resonant surface

$$\omega_{\boldsymbol{k_1}} + \omega_{\boldsymbol{k_2}} = \omega_{\boldsymbol{k_3}} + \omega_{\boldsymbol{k_4}} \tag{2}$$

$$\boldsymbol{k_1} + \boldsymbol{k_2} = \boldsymbol{k_3} + \boldsymbol{k_4} \tag{3}$$

The accuracy advantage of knowing the analytical expression for the S_{nl} term, known in physical oceanography as XNL, is overshadowed by its computational complexity. Today, none of the operational wave forecasting models can afford performing XNL computations in real time. Instead, the operational approximation, known as the DIA and its derivatives, are used to approximate this source term.. The implication of such simplification is the inclusion of a tuning coefficient in front of nonlinear term; however, several publications have now shown that the DIA does not provide a good approximation of the actual form of XNL. Consequently, other source terms must be adjusted to allow the model Eq.(1) to obtain desirable results.

In contrast to S_{nl}, the knowledge of the S_{in} and S_{diss} source terms is poor, and both now include many heuristic factors and coefficients.

The creation of a reliable, well justified theory of S_{in} has been hindered by strong turbulent fluctuations in boundary layer over the sea surface. Even one of the most crucial elements of this theory, the vertical distribution of horizontal wind velocity in the region closest to the ocean surface, where wave motions strongly interact with atmospheric motions, is still the subject of the debate. The history of the development of different wind input forms is full of assumptions, which fundamentally restrict the magnitude and directional distribution of this surface term. As a result, the values of different wind input terms scatter by a factor of $300 \div 500\%$ (Badulin et al., 2005; Pushkarev and Zakharov, 2016). Additional information on this detailed analysis of current state of wind input terms can be found in Pushkarev and Zakharov (2016).

Similar to the wind input term, there is little consent on the parameterization of the source dissipation term S_{diss}. The physical dissipation mechanism, which most physical oceanographers agree on, is the effect of wave energy loss due to wave breaking, while there are also other dubious ad-hoc "long wave" dissipation source terms, having heuristically justified physical explanations. Currently, there is not even an agreement on the localization of wave breaking events in Fourier space. The approach currently utilized in operational wave forecasting models mostly relies on the dissipation, localized in the vicinity of the spectral energy peak. Recent numerical experiments show (Pushkarev and Zakharov, 2016; Dyachenko et al., 2015; Zakharov et al., 2009), however, that such approach does not pass most of the tests associated with the essentially nonlinear nature of the Eq.(1).

Wave breaking dissipation, known also as "white-capping dissipation", is an important physical phenomenon, not properly studied yet for the reasons of mathematical and technological complexity. Longuet-Higgins (1980a, b) achieved important results, but didn't accomplish the theory completely. Irisov and Voronovich (2011) studied wave-breaking of the short waves, "squeezed" by surface currents, caused by longer waves, and showed that they become steep and unstable. Our explanation is simpler, but has the same consequences: the "wedge" formation, preceding the wave breaking, causes the "fat tail" appearance in Fourier space. Subsequent smoothing of the tip of the wedge is equivalent to the "chopping off" of the developed high-frequency tail – a sort of natural low-pass filtering – leading to the loss of the wave energy. This effect is referred as "cigar cutting effect" (Pushkarev and Zakharov, 2016). Both scenarios have the same consequences of wave surface smoothing, and are indirectly confirmed by presented numerical experiments in that study.

Instead of following the previous path of time-consuming numerical and field experiments, the authors of the current manuscript are pursuing an alternative approach to definition of S_{in} and S_{diss} terms . Based on the leading nonlinearity role in Eq.(1) ((Zakharov, 2010; Zakharov and Badulin, 2011)), it was decided to analyze a multi-parametric family of self-similar

solutions of Eq.(1). The comparison with the results of field observations allowed to find a new wind input form, herein termed the ZRP S_{in} wind input source term (Zakharov et al., 2012). The wave breaking dissipation term S_{diss} has been chosen in the form of "implicit dissipation" via Phillips $\sim f^{-5}$ spectral continuation tail. That framework reproduced the observations of a dozen of field experiments , i.e. self-similar exponents $p = 1$ and $q = -0.3$ of power dependencies of total wave energy $\sim \chi^p$ and spectral peak frequency $\sim \omega^q$ along a fetch (Pushkarev and Zakharov, 2016).

In the following section we are describing the details of ZRP model and pertaining numerical results in time domain and duration limited statements.

2 Experimental evidence

Here we examine the empirical evidence from around the world, which has been utilized to quantify energy levels within the equilibrium spectral range by Resio et al. (2004a). For convenience, we shall also use the same notation used by Resio et al. (2004a) in their study, for the angular averaged spectral energy densities in frequency and wavenumber spaces:

$$E_4(f) = \frac{2\pi\alpha_4 V g}{(2\pi f)^4} \tag{4}$$

$$F_4(k) = \beta k^{-5/2} \tag{5}$$

where $f = \frac{\omega}{2\pi}$, α_4 is the constant, V is some characteristic velocity and $\beta = \frac{1}{2}\alpha_4 V g^{-1/2}$. These notations are based on relation of spectral densities $E(f)$ and $F(k)$ in frequency $f = \frac{\omega}{2\pi}$ and wave-number k bases:

$$F(k) = \frac{c_g}{2\pi} E(f) \tag{6}$$

where $c_g = \frac{d\omega}{dk} = \frac{1}{2\cdot 2\pi}\frac{g}{f}$ is the group velocity.

The notations in Eqs.(4)-(5) are connected with the spectral energy density $\epsilon(\omega, \theta)$ through

$$E(f) = 2\pi \int \epsilon(\omega, \theta) d\theta \tag{7}$$

The Resio et al. (2004a) analysis showed that experimental energy spectra $F(k)$, estimated through averaging $< k^{5/2} F(k) >$, can be approximated by linear regression line as the function of $(u_\lambda^2 c_p)^{1/3} g^{-1/2}$. Fig.1 shows that the regression line

$$\beta = \frac{1}{2}\alpha_4 \left[(u_\lambda^2 c_p)^{1/3} - u_0 \right] g^{-1/2} \tag{8}$$

indeed, seems to be a reasonable approximation of these observations.

Here $\alpha_4 = 0.00553$, $u_0 = 1.93\ m/sec$, c_p is the spectral peak phase speed and u_λ is the wind speed at the elevation equal to a fixed fraction $\lambda = 0.065$ of the spectral peak wavelength $2\pi/k_p$, where k_p is the spectral peak wave number. It is important to emphasize that Resio et al. (2004a) experiments show that parameter β increases with development of the wind-driven sea, when f_p decreases and C_p increases. This observation is consistent with the weak turbulent theory, where $\beta \sim P^{1/3}$ (Zakharov et al., 1992); here P is the wave energy flux toward small scales.

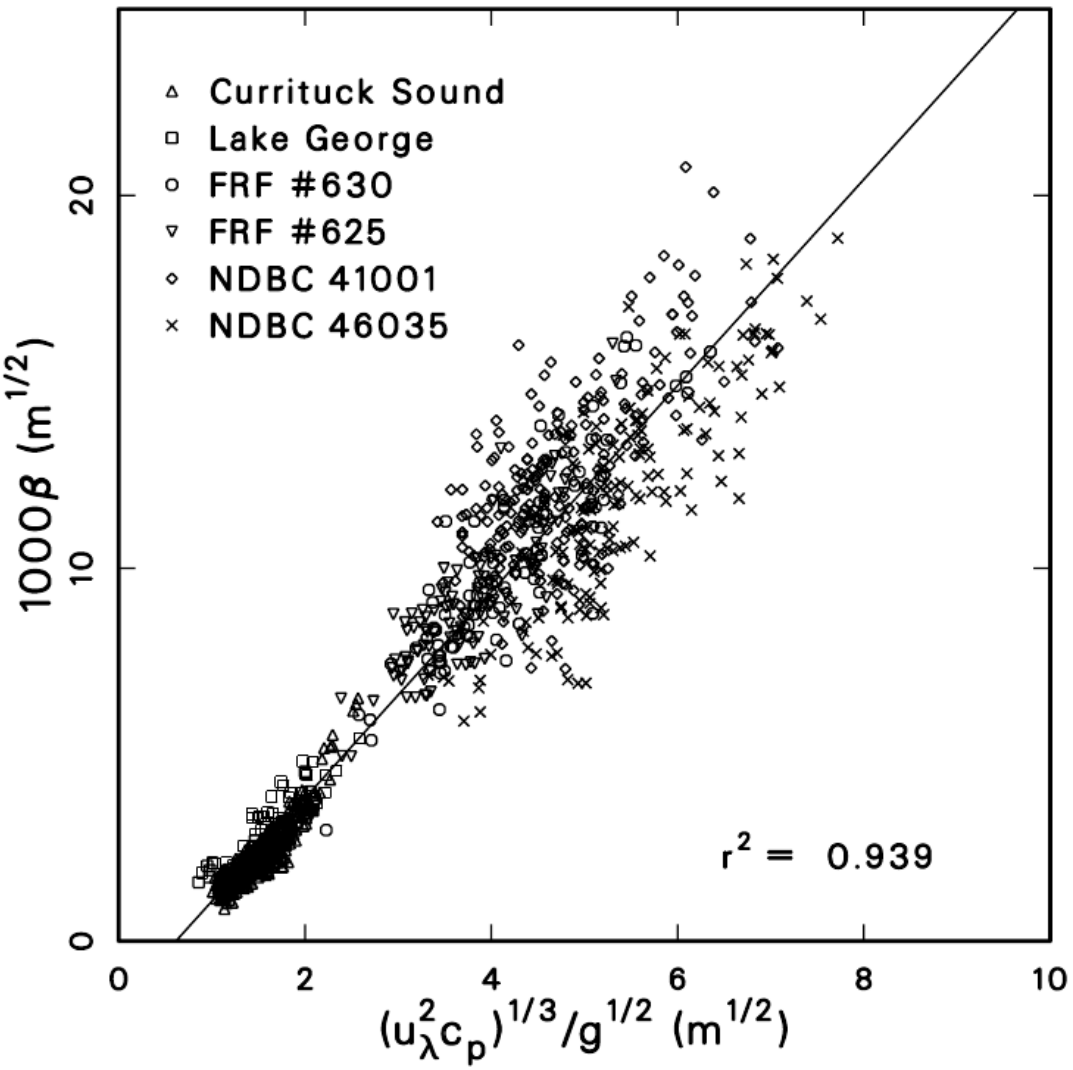

Figure 1. Correlation of equilibrium range coefficient β with $(u_\lambda^2 c_p)^{1/3}/g^{1/2}$ based on data from six disparate sources. Adapted from Resio et al. (2004a)

Resio et al. (2004a) assumed that the near surface boundary layer can be treated as neutral and thus follows a conventional logarithmic profile

$$u_\lambda = \frac{u_\star}{\kappa} \ln \frac{z}{z_0} \tag{9}$$

having Von Karman coefficient $\kappa = 0.41$, where $z = \lambda \cdot 2\pi/k_p$ is the elevation equal to a fixed fraction $\lambda = 0.065$ of the spectral peak wavelength $2\pi/k_p$, where k_p is the spectral peak wave number, and $z_0 = \alpha_C u_\star^2/g$ subject to Charnock (1955) surface roughness with $\alpha_C = 0.015$.

3 Theoretical considerations

Self-similar solutions consistent with the conservative kinetic equation

$$\frac{\partial \epsilon(\omega,\theta)}{\partial t} = S_{nl} \tag{10}$$

were studied in Zakharov (2005), Badulin et al. (2005). In this section we study self-similar solutions of the forced kinetic equation

$$\frac{\partial \epsilon(\omega,\theta)}{\partial t} = S_{nl} + \gamma(\omega,\theta)\epsilon(\omega,\theta) \tag{11}$$

where $\epsilon(\omega,\theta) = \frac{2\omega^4}{g} N(\mathbf{k},\theta)$ is the energy spectrum. For our purposes, it is sufficient to simply use the dimensional estimate for S_{nl},

$$S_{nl} \simeq \omega \left(\frac{\omega^5 \epsilon}{g^2}\right)^2 \epsilon \tag{12}$$

Eq.(11) has a self-similar solution if

$$\gamma(\omega,\theta) = \alpha \omega^{1+s} f(\theta) \tag{13}$$

where s is a constant. Looking for self-similar solution in the form

$$\epsilon(\omega,t) = t^{p+q} F(\omega t^q) \tag{14}$$

we find

$$q = \frac{1}{s+1} \tag{15}$$

$$p = \frac{9q-1}{2} = \frac{8-s}{2(s+1)} \tag{16}$$

The function $F(\xi)$ has the maximum at $\xi \sim \xi_p$, thus the frequency of the spectral peak is

$$\omega_p \simeq \xi_p t^{-q} \tag{17}$$

The phase velocity at the spectral peak is

$$c_p = \frac{g}{\omega_p} = \frac{g}{\xi_p} t^q = \frac{g}{\xi_p} t^{\frac{1}{s+1}} \tag{18}$$

According to experimental data, the main energy input into the spectrum occurs in the vicinity of the spectral peak, i.e. at $\omega \simeq \omega_p$. For $\omega >> \omega_p$, the spectrum is described by Zakharov-Filonenko tail

$$\epsilon(\omega) \sim P^{1/3} \omega^{-4} \tag{19}$$

Here

$$P = \int_0^\infty \int_0^{2\pi} \gamma(\omega,\theta)\epsilon(\omega,\theta) d\omega d\theta \tag{20}$$

This integral converges if $s < 2$. For large ω

$$\epsilon(\omega,t) \simeq \frac{t^{p-3q}}{\omega^4} \simeq \frac{t^{\frac{2-s}{2(s+1)}}}{\omega^4} \tag{21}$$

More accurately

$$\epsilon(\omega,t) \simeq \frac{\mu g}{\omega^4} u^{1-\eta} c_p^{\eta} g(\theta) \tag{22}$$

$$\eta = \frac{2-s}{2} \tag{23}$$

Now supposing $s = 4/3$ and $\gamma \simeq \omega^{7/3}$, we get $\eta = 1/3$, which is exactly experimental regression line prediction. Because it is known from regression line in Fig.1 that $\xi = 1/3$, we immediately get $s = 4/3$ and the wind input term

$$S_{wind} \simeq \omega^{7/3} \epsilon \tag{24}$$

Another important theoretical relationship, that can be derived from joint consideration of Eqs. (4), (6) and (22) is

$$1000\beta = \lambda \frac{(u^2 c_p)^{1/3}}{g^{1/2}} \tag{25}$$

which shows a theoretical equivalence to the experimental regression, where λ is an unknown constant, defined experimentally.

At the end of the section, we present the summary of important relationships.

Wave action N, energy E and momentum M in frequency-angle presentation are:

$$N = \frac{2}{g^2} \int_0^{\infty} \int_0^{2\pi} \omega^3 n d\omega d\phi \tag{26}$$

$$E = \frac{2}{g^2} \int_0^{\infty} \int_0^{2\pi} \omega^4 n d\omega d\phi \tag{27}$$

$$M = \frac{2}{g^3} \int_0^{\infty} \int_0^{2\pi} \omega^5 n \cos\phi d\omega d\phi \tag{28}$$

The self-similar relations for duration limited case:

$$\epsilon = t^{p+q} F(\omega t^q) \tag{29}$$

$$9q - 2p = 1, \ p = 10/7, \ q = 3/7 \ \ s = 4/3 \tag{30}$$

$$N \sim t^{p+q} \tag{31}$$

$$E \sim t^{p} \tag{32}$$

$$M \sim t^{p-q} \tag{33}$$

$$< \omega > \sim t^{-q} \tag{34}$$

The same sort of self-similar analysis gives self-similar relations for fetch limited case:

$$\epsilon = \chi^{p+q} F(\omega\chi^q) \tag{35}$$

$$10q - 2p = 1,\ p = 1,\ q = 3/10\ \ s = 4/3 \tag{36}$$

$$N \sim \chi^{p+q} \tag{37}$$

$$E \sim \chi^{p} \tag{38}$$

$$M \sim \chi^{p-q} \tag{39}$$

$$<\omega> \sim \chi^{-q} \tag{40}$$

4 Numerical validation of relationship

To check the self-similar hypothesis posed in Eq.(24), we performed a series of numerical simulations of Eq.(1) in the spatially homogeneous time domain $\frac{\partial N}{\partial \boldsymbol{r}} = 0$ and spatially inhomogeneous fetch limited $\frac{\partial N}{\partial t} = 0$ situations.

All simulations used WRT (Webb-Resio-Tracy) method (see Tracy and Resio (1982)), which calculates the nonlinear interaction term in the exact form. The presented numerical simulation utilized the version of WRT method, previously used in Korotkevich et al. (2008); Resio and Perrie (1989); Perrie and Zakharov (1999); Resio et al. (2004b); Long and Resio (2007); Badulin and Zakharov (2012); Webb (1978), and used the grid of 71 points in frequency and 36 points in angle domains.

The constant wind of speed $10\ m/sec$ was assumed blowing away from the shore line, along the fetch. The assumption of the constant wind speed is a necessary simplification, due to the fact that the numerical simulation is being compared to various data from field experiments, and the considered set-up is the simplest physical situation, which can be modeled.

The same ZRP wind input term Eq.(24) has been used in both cases in the form

$$S_{in}(\omega,\phi) = \gamma(\omega,\phi)\cdot\varepsilon(\omega,\phi) \tag{41}$$

$$\gamma = 0.05\frac{\rho_{air}}{\rho_{water}}\omega\left(\frac{\omega}{\omega_0}\right)^{4/3} f(\theta) \tag{42}$$

$$f(\theta) = \begin{cases} \cos^2\theta \ \text{ for } -\pi/2 \le \theta \le \pi/2 \\ 0 \ \text{ otherwise} \end{cases} \tag{43}$$

$$\omega_0 = \frac{g}{u_{10}},\ \frac{\rho_{air}}{\rho_{water}} = 1.3\cdot 10^{-3} \tag{44}$$

where u_{10} is the wind speed, ρ_{air} and ρ_{water} are the air and water density correspondingly. It is conceivable to use more sophisticated expression for $f(\theta)$, for instance $f(\theta) = q(\theta) - q(0)$. The wind speed u_{10} is taken here as the speed at a reference level of 10 meters. To make a direct comparison with experimental results of Resio et al. (2004a), we used the relation $u_\star \simeq u_{10}/28$ (see Golitsyn (2010)) in Eq.(9).

Both situations also need the knowledge of the dissipation term S_{diss}, which is taken into account in the "implicit" form (see Pushkarev and Zakharov (2016)), where white-capping dissipation was included through f^{-5} energy spectral tail stretching in

frequency range from $f_d = 1.1$ to $f_{max} = 2.0$. To date, this approach has been confirmed by both experimental observations and numerical experiments to provide an effective direct cascade energy sink at high frequencies.

Next, we specifically stop on the details of the “implicit" high-frequency damping.

4.1 The details of "implicit"dissipation

The “implicit" damping consists in continuation of the spectral tail by Phillips law (see Phillips (1966)) $A(\omega_{crit}) \cdot \omega^{-5}$, where $A(\omega_{crit})$ is the parameter dynamically changing in time.

The coefficient $A(\omega_{crit})$, in front of ω^{-5}, is not well known from theory, but is not required to be defined in an explicit form. Instead, it is dynamically determined from the continuity condition of the spectrum, at frequency ω_{crit}, on every time step. In other words, the starting point of the Phillips spectrum coincides with the last point of the dynamically changing spectrum, at the frequency point $\omega_{crit} = 2\pi f_{crit}$, where $f_{crit} \simeq 1.1\ Hz$, as per Resio and Long experimental observations, see Long and Resio (2007). This is the way the high frequency “implicit" damping is incorporated into the alternative computational framework of HE.

One should note recently developed analytical models, which automatically describe the transition from the KZ spectrum ω^{-4} to Phillips tail ω^{-5}, see Badulin and Zakharov (2012). Such modification of the “implicit" damping is in future plans, but the question of the finer details of the high-frequency “implicit" damping structure is of secondary importance, at the current “proof of the concept" stage.

4.2 Time domain simulation

All time domain numerical simulations shown here have been started from uniform noise energy distribution in Fourier space with a small initial wave height.

Fig.2 shows the total energy growth as a function of time close to self-similar prediction Eq.(32) for $p = 10/7$, see Fig.3.

The dependence of mean frequency, on the fetch, shown in Fig.4 demonstrates good correspondence with self-similar dependence found in Eq.(34), for $q = 3/7$ (Fig.5).

The check of consistency with the “magic number” $(9q - 2p)$, as defined in (Pushkarev and Zakharov, 2016), is presented in Fig.6. This also agrees with the self-similar prediction in Eq.30.

Fig.7 presents angle-integrated energy spectrum, as the function of frequency, in logarithmic coordinates. One can see that it consists of the segments of:

- spectral peak region
- equilibrium range ω^{-4}
- Phillips high frequency tail ω^{-5}

The compensated spectrum $F(k) \cdot k^{5/2}$ is presented in Fig.9. One can see plateau-like region responsible for $k^{-5/2}$ behavior, equivalent to ω^{-4} tail in Fig.7. This exact solution of Eq.(10), known as KZ spectrum, was found by Zakharov and Filonenko

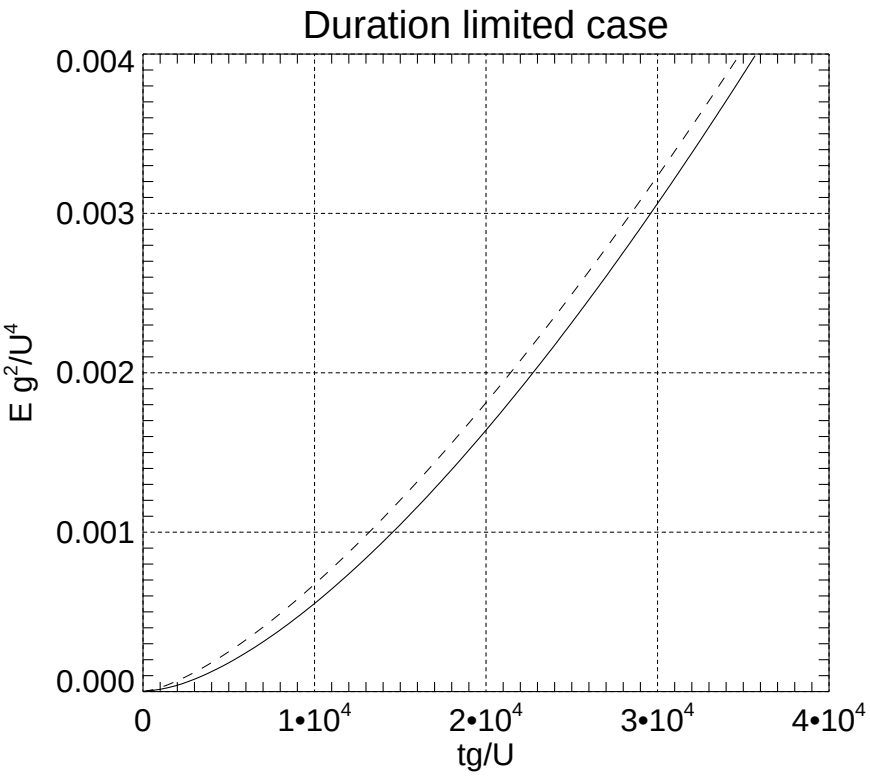

Figure 2. Dimensionless energy Eg^2/U^4 versus dimensionless time tg/U for duration limited case. Dashed fit $1.3 \cdot 10^{-9} \, (tg/U)^{10/7}$

(1967). The universality of ω^{-4} asymptotic for large frequency has been observed in multiple experimental field observations and is accepted by the oceanographic community after the seminal work of Phillips (1985). One should note that most of the energy flux into the system comes in the vicinity of the spectral peak, as shown in Fig.8, providing significant inertial interval for KZ spectrum.

The angular spectral distribution of energy, presented in Fig.10, is consistent with the results of experimental observations that show a broadening of the angular spreading in both directions away from the spectral peak frequency.

To compare the time domain numerical simulation results with the experimental analysis by Resio et al. (2004a), presented in Fig.1, Fig.11 shows the function $\beta = F(k) \cdot k^{5/2}$ as a function of $(u_\lambda^2 C_p)^{1/3}/g^{1/2}$ for wind speed $u_{10} = 10.0$ m/sec, along with the regression line from Resio et al. (2004a) and theoretical prediction Eq.(25) for $\lambda = 2.74$. The numerical results and theoretical prediction line fall within RMS deviation from the regression line.

4.3 Limited fetch numerical simulations

The limited fetch simulation was performed within the framework of the stationary version of the Eq.(1):

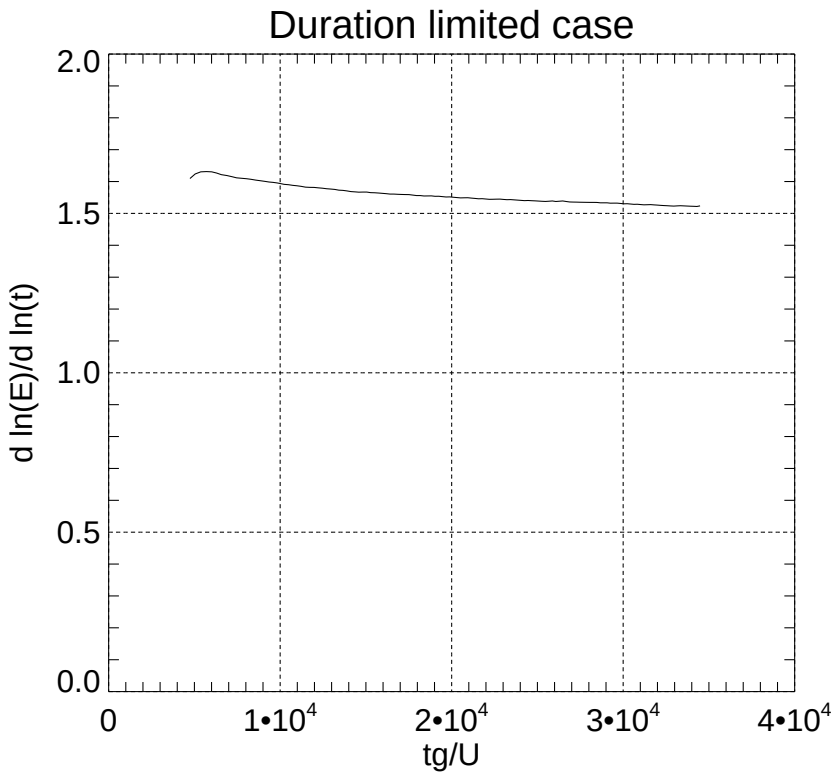

Figure 3. Local energy exponent power $p = \frac{d\ln E}{d\ln t}$ as a function of dimensionless time tg/U for duration limited case.

$$\frac{1}{2}\frac{g\cos\theta}{\omega}\frac{\partial\epsilon}{\partial x} = S_{nl}(\epsilon) + S_{wind} + S_{diss} \tag{45}$$

where x is the coordinate orthogonal to the shore and θ is the angle between individual wavenumber $\boldsymbol{k}$ and the axis $\boldsymbol{x}$.

Stationarity in Eq.(45) is somewhat difficult for numerical simulation, since it contains the singularity in the form of $\cos\theta$ in front of $\frac{\partial\epsilon}{\partial x}$. This problem was overcome by zeroing one half of the Fourier space of the system for the waves propagating toward the shore. Since the energy in such waves is small with respect to waves propagating in the offshore direction, such an approximation is quite reasonable for our purposes.

Since the wind forcing index s in the fetch-limited case is similar to that in the time domain, the numerical simulation of Eq.(45) has been performed for the same input functions as in the time domain case with the same low-level energy noise initial conditions in Fourier space.

Fig.12 shows total energy growth as a function of fetch coordinate close to self-similar prediction Eq.(38) for $p = 1$, see Fig.13.

Dependence of mean frequency on the fetch, shown in Fig.14, demonstrates good correspondence with self-similar dependence Eq.(34), for $q = 3/10$ (Fig.15).

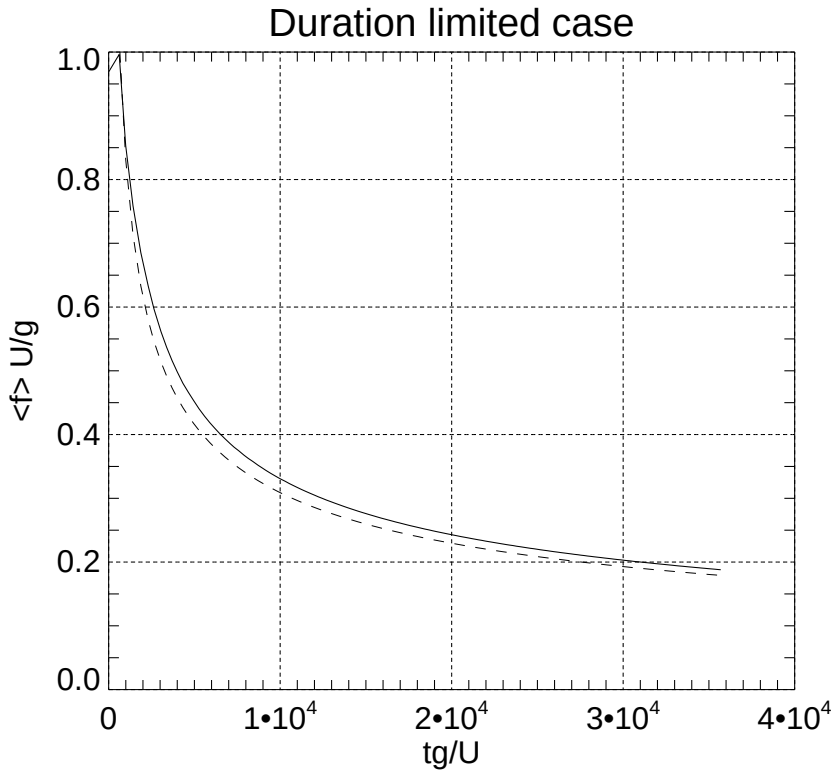

Figure 4. Dimensionless frequency $< f > \cdot U/g = E/N \cdot U/g$ versus dimensionless time tg/U for duration limited case, dashed fit by $16.0 \cdot (tg/U)^{-3/7}$.

The check of "magic number" $(10q - 2p)$ is presented in Fig.16 and agrees with the self-similar prediction of Eq.36.

Fig.17 presents directionally integrated energy spectrum, as the function of frequency, in logarithmic coordinates. As in the time domain case, one can see that it consists of the segments of:

- spectral peak region
- equilibrium range ω^{-4}
- Phillips high frequency tail ω^{-5}

The compensated spectrum $F(k) \cdot k^{5/2}$ is presented in Fig.19. One can see plateau-like region responsible for $k^{-5/2}$ behavior, equivalent to ω^{-4} tail in Fig.17. As in the time domain case, KZ solution (Zakharov and Filonenko, 1967) also holds for limited domain case, and most of the energy flux into the system comes in the vicinity of the spectral peak as well, as shown in Fig.18, providing significant inertial interval for KZ spectrum.

The angular spectrum distribution, consistent with the broadening of the spectrum in experimental observations, is presented in Fig.20.

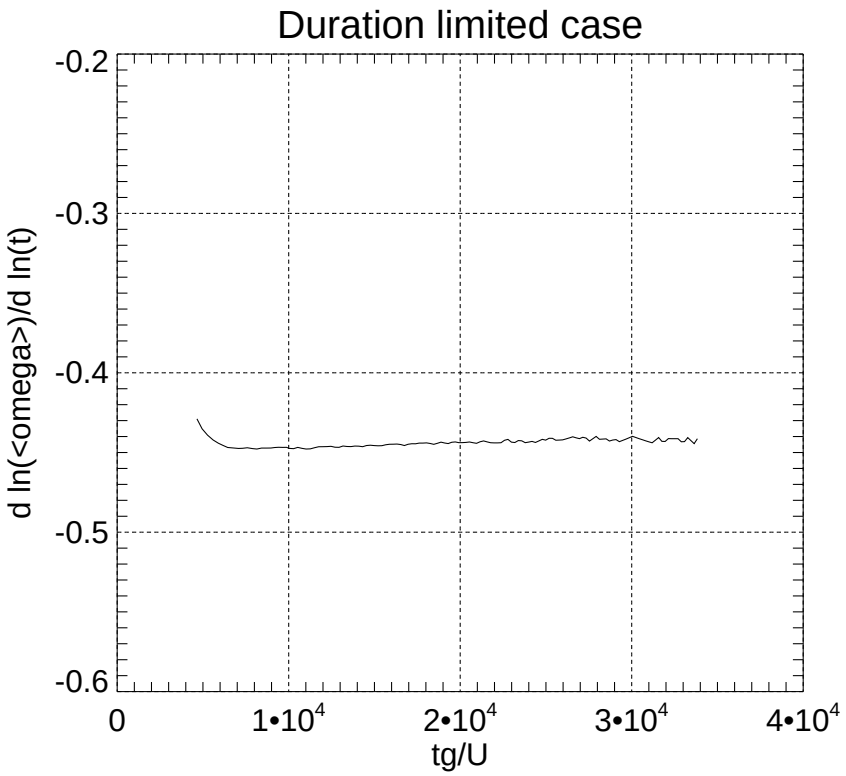

Figure 5. Local mean frequency exponent power $q = \frac{d\ln<\omega>}{d\ln t}$ as a function of dimensionless time tg/U for duration limited case.

To compare the limited fetch numerical simulation results with the experimental analysis by Resio et al. (2004a), presented in Fig.1, Fig.21 shows the function $\beta = F(k) \cdot k^{5/2}$ as a function of $(u_\lambda^2 C_p)^{1/3}/g^{1/2}$ for wind speed $u_{10} = 10.0$ m/sec, along with the regression line from Resio et al. (2004a) and its theoretical prediction Eq.(25) for $\lambda = 2.11$. The numerical results and theoretical prediction line fall into RMS deviation from the regression line.

5 Comparison with the experiments

The comparison of limited fetch and time domain simulations with the experimental results by Resio and Long (2007) and theoretical prediction Eq.(8) is presented in Fig.11 and Fig.21. One should note that the numerical results and theoretical prediction line with corresponding values of λ fall into RMS deviation from the experimental regression line Eq.(8).

The dimensionless energy ε and frequency ω dependencies on the dimensionless fetch χ for the limited fetch simulation, superimposed on the experimental observations collected by Young (1999), are presented of Fig.22 and Fig.23. One should note quite good correspondence of the presented numerical results with these experimental observations.

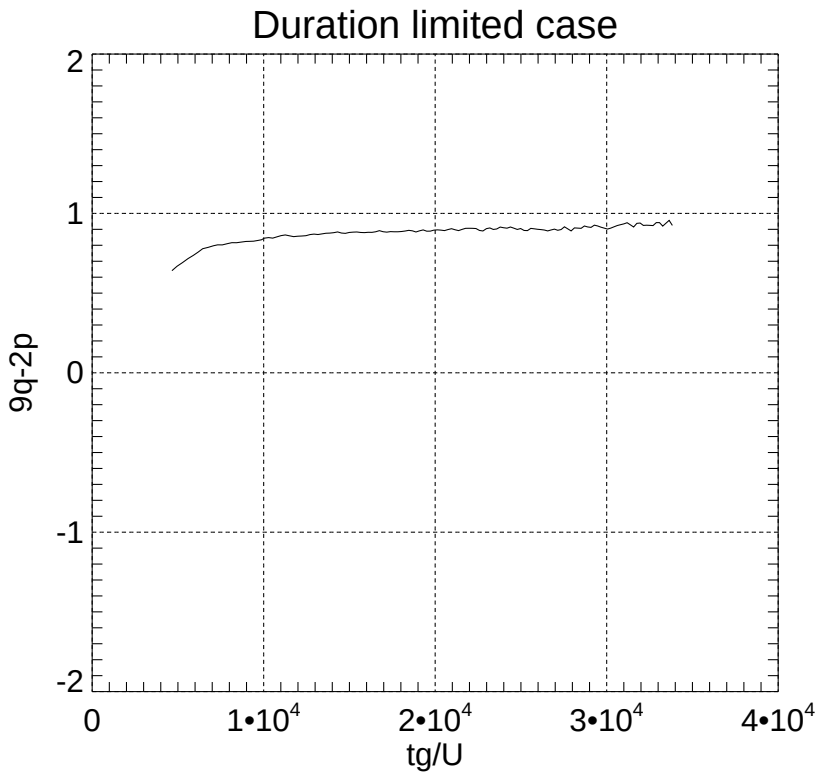

Figure 6. "Magic number" $9q - 2p$ as a function of dimensionless time tg/U for duration limited case.

6 Conclusions

We analyzed the new ZRP form for wind input, proposed in Zakharov et al. (2012). Both numerical simulations for time domain and limited fetch cases, which used ZRP wind input term, XNL nonlinear term S_{nl} and "implicit" high-frequency dissipation, shown good agreement with predicted self-similar properties of Hasselmann equation, experimentally obtained regression line Resio et al. (2004a); Resio and Long (2007) and its theoretical prediction. The authors of the research hope that this new framework will offer additional guidance for the source terms in operational models .

Acknowledgements. The research presented in section 4.2 has been accomplished due to support of the grant "Wave turbulence: the theory, mathematical modeling and experiment" of the Russian Scientific Foundation No 14-22-00174. The research presented in other chapters was supported by ONR grant N00014-10-1-0991. The authors gratefully acknowledge the support of these foundations.

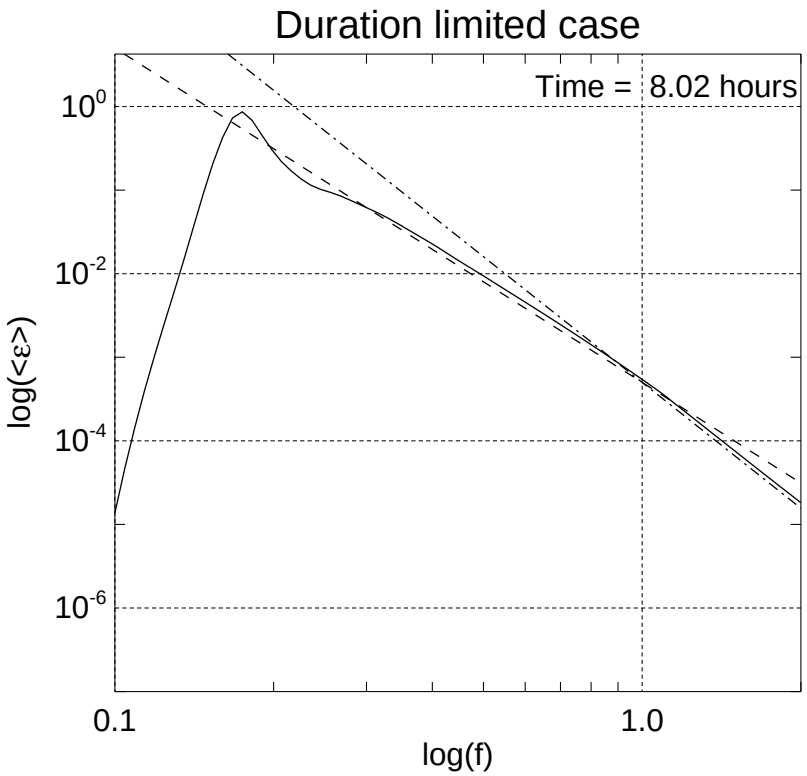

Figure 7. Decimal logarithm of the angle averaged spectrum as a function of the decimal logarithm of the frequency for duration limited case.

References

Badulin, S. I. and Zakharov, V. E.: The generalized Phillips' spectra and new dissipation function for wind-driven seas, arXiv:1212.0963 [physics.ao-ph], pp. 1 – 16, 2012.

Badulin, S. I., Pushkarev, A. N., D.Resio, and Zakharov, V. E.: Self-similarity of wind-driven sea, Nonlinear Proc. in Geophysics, 12, 891 – 945, 2005.

Charnock, H.: Wind stress on a water surface, Q.J.R. Meteorol. Soc., 81, 639 – 640, 1955.

Dyachenko, A. I., Kachulin, D. I., and Zakharov, V. E.: Evolution of one-dimensional wind-driven sea spectra, JETP Letters, 102, 577 – 581, 2015.

Golitsyn, G.: The Energy Cycle of Wind Waves on the Sea Surface, Izvestiya, Atmospheric and Oceanic Physics, 46, 6–13, 2010.

Hasselmann, K.: On the non-linear energy transfer in a gravity-wave spectrum. Part 1. General theory, Journal of Fluid Mechanics, 12, 481 – 500, 1962.

Hasselmann, K.: On the non-linear energy transfer in a gravity wave spectrum. Part 2. Conservation theorems; wave-particle analogy; irrevesibility, Journal of Fluid Mechanics, 15, 273 – 281, 1963.

Irisov, V. and Voronovich, A.: Numerical Simulation of Wave Breaking, Journal of Physical Oceanography, 41, 346 – 364, 2011.

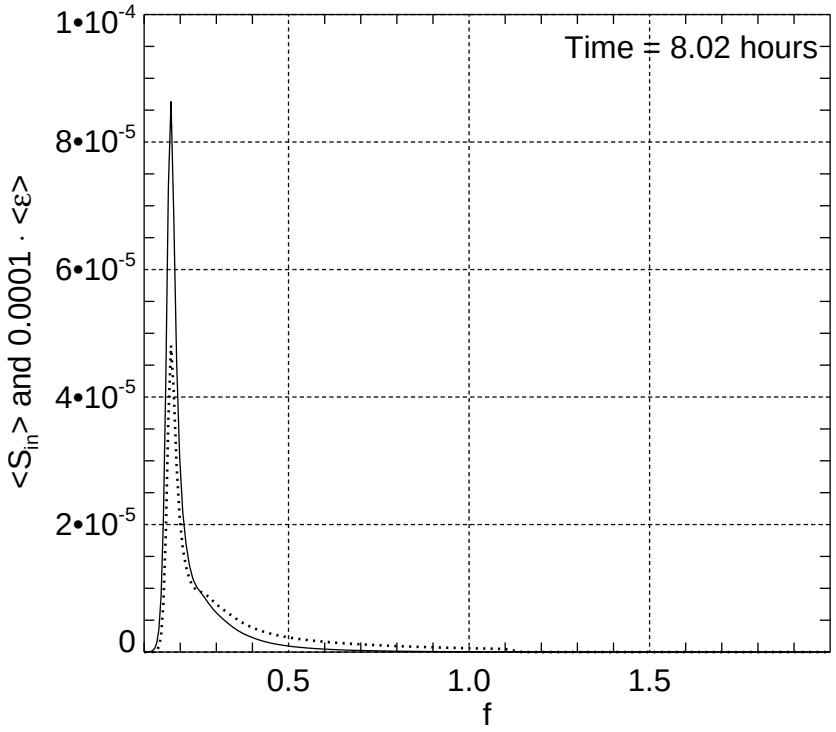

Figure 8. Typical, angle averaged, wind input function density $< S_{in} >= \frac{1}{2\pi}\int \gamma(\omega,\theta)\varepsilon(\omega,\theta)d\theta$ and angle averaged spectrum $< \varepsilon >= \frac{1}{2\pi}\int \varepsilon(\omega,\theta)d\theta$ (solid line) as the functions of the frequency $f = \frac{\omega}{2\pi}$.

Korotkevich, A. O., Pushkarev, A. N., Resio, D., and Zakharov, V. E.: Numerical verification of the weak turbulent model for swell evolution, Eur. J. Mech. B - Fluids, 27, 361 – 387, 2008.

Long, C. and Resio, D.: Wind wave spectral observations in Currituck Sound, North Carolina, JGR, 112, C05 001, 2007.

Longuet-Higgins, M. S.: A technique for time-dependent, free-surface flow, Proc.R.Soc.Lond. A, 371, 441 – 451, 1980a.

Longuet-Higgins, M. S.: On the forming of sharp corners at a free surface, Proc.R.Soc.Lond. A, 371, 453 – 478, 1980b.

Nordheim, L. W.: On the Kinetic Method in the New Statistics and Its Application in the Electron Theory of Conductivity, Proc. R. Soc. Lond. A, 119, 689 – 698, 1928.

Perrie, W. and Zakharov, V. E.: The equilibrium range cascades of wind-generated waves, Eur. J. Mech. B/Fluids, 18, 365 – 371, 1999.

Phillips, O. M.: The dynamics of the upper ocean, Cambridge monographs on mechanics and applied mathematics, Cambridge U.P., 1966.

Phillips, O. M.: Spectral and statistical properties of the equilibrium range in wind-generated gravity waves, Journal of Fluid Mechanics, pp. 505 – 531, 1985.

Pushkarev, A. and Zakharov, V.: Limited fetch revisited: comparison of wind input terms, in surface wave modeling, Ocean Modeling, 103, 18 — 37, doi:10.1016/j.ocemod.2016.03.005, 2016.

Resio, D. and Perrie, W.: Implications of an f^{-4} equilibrium range for wind-generated waves, JPO, 19, 193 – 204, 1989.

Resio, D. T. and Long, C. E.: Wind wave spectral observations in Currituck Sound, North Carolina, J. Geophys. Res., 112, C05 001, 2007.

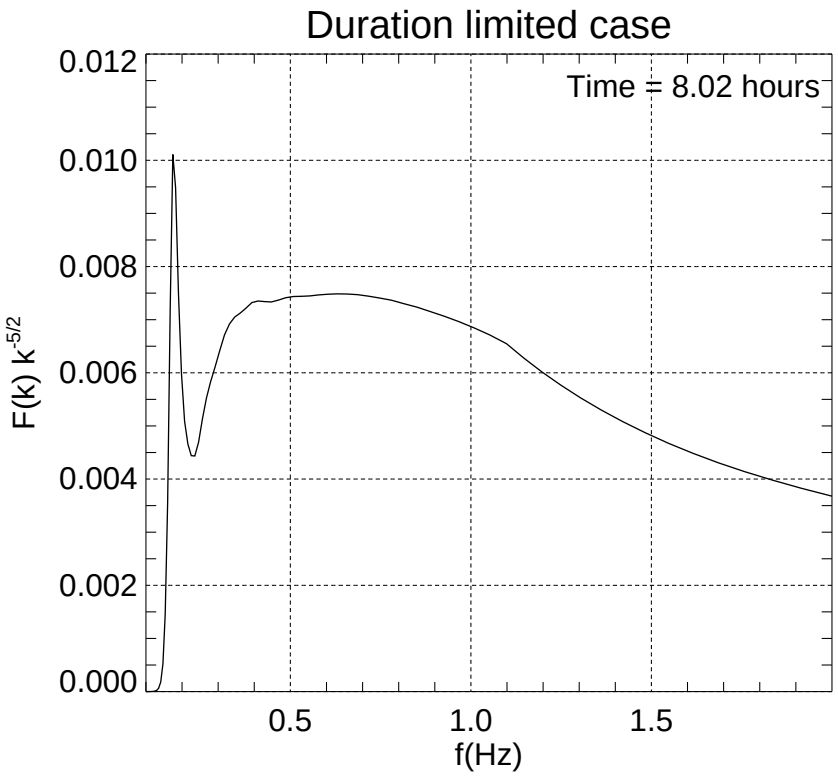

Figure 9. Compensated spectrum for duration limited case as a function of linear frequency f.

Resio, D. T. and Perrie, W.: A numerical study of nonlinear energy fluxes due to wave-wave interactions in a wave spectrum. Part I: Methodology and basic results, J. Fluid Mech., 223, 603 – 629, 1991.

Resio, D. T., Long, C. E., and Vincent, C. L.: Equilibrium-range constant in wind-generated wave spectra, J. Geophys. Res., 109, C01 018, 2004a.

Resio, D. T., Long, C. E., and Vincent, C. L.: Equilibrium-range constant in wind-generated wave spectra, JGR, 109, CO1018, 2004b.

SWAN: http://swanmodel.sourceforge.net/, 2015.

Tolman, H. L.: User manual and system documentation of WAVEWATCH III, Environmental Modeling Center, Marine Modeling and Analysis Branch, 2013.

Tracy, B. and Resio, D.: Theory and calculation of the nonlinear energy transfer between sea waves in deep water, WES report 11, U.S. Army Engineer Waterways Experiment Station, Vicksburg, MS, 1982.

Webb, D. J.: Non-linear transfers between sea waves, Deep-Sea Res., 25, 279 – 298, 1978.

Young, I. R.: Wind Generated Ocean Waves, Elsevier, 1999.

Zakharov, V. E.: Theoretical interpretation of fetch-limited wind-driven sea observations, NPG, 13, 1 – 16, 2005.

Zakharov, V. E.: Energy balances in a wind-driven sea, Physica Scripta, T142, 014 052, 2010.

Zakharov, V. E. and Badulin, S. I.: On energy balance in wind-driven sea, Doklady Akademii Nauk, 440, 691 – 695, 2011.

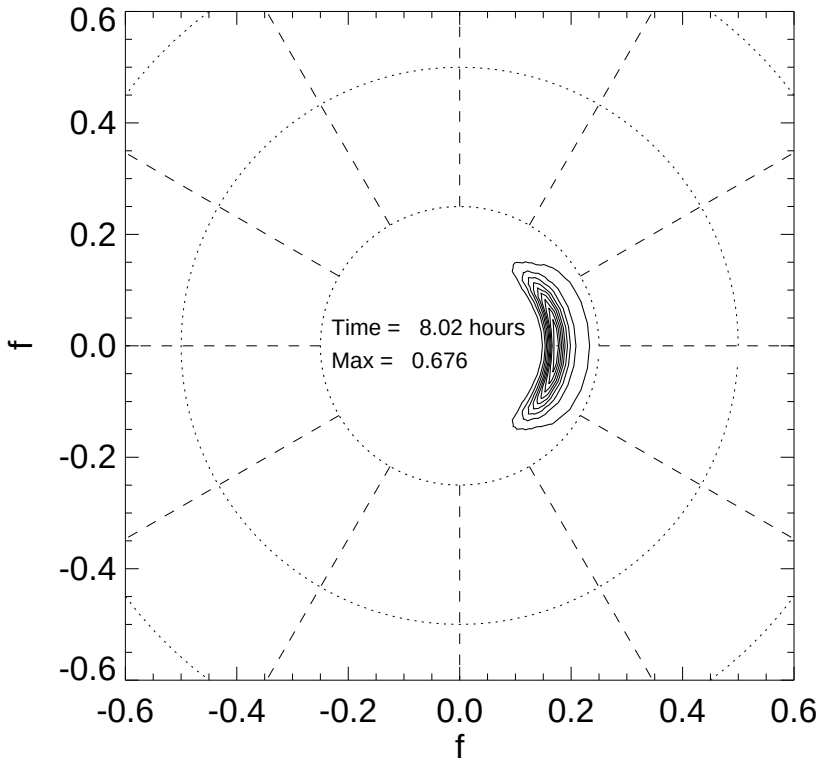

Figure 10. Angular spectra dependence for duration limited case.

Zakharov, V. E. and Filonenko, N. N.: The energy spectrum for stochastic oscillation of a fluid's surface, Dokl.Akad.Nauk., 170, 1992 – 1995, 1966.

Zakharov, V. E. and Filonenko, N. N.: The energy spectrum for stochastic oscillations of a fluid surface, Sov. Phys. Docl., 11, 881 – 884, 1967.

Zakharov, V. E., L'vov, V. S., and Falkovich, G.: Kolmogorov Spectra of Turbulence I: Wave Turbulence, Springer-Verlag, 1992.

Zakharov, V. E., Korotkevich, A. O., and Prokofiev, A. O.: On Dissipation Function of Ocean Waves due to Whitecapping, in: American Institute of Physics Conference Series, edited by Simos, T. E., G.Psihoyios, and Tsitouras, C., vol. 1168, pp. 1229 – 1237, 2009.

Zakharov, V. E., Resio, D., and Pushkarev, A.: New wind input term consistent with experimental, theoretical and numerical considerations, http://arxiv.org/abs/1212.1069/, 2012.

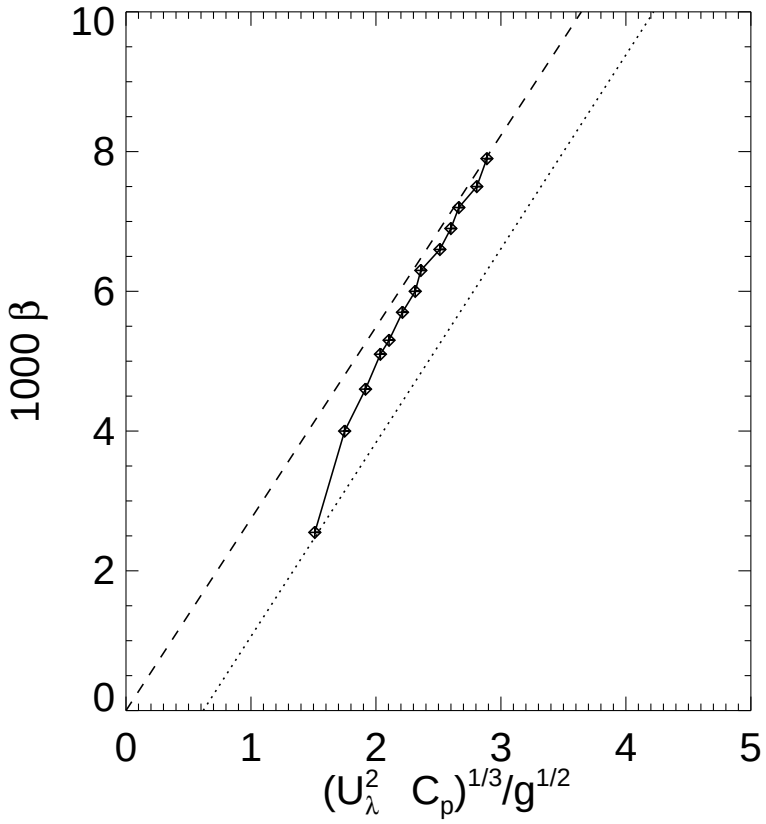

Figure 11. Experimental, theoretical and numerical evidence of dependence of 1000β on $\left(u_\lambda^2 c_p\right)^{1/3}/g^{1/2}$. Dashed line - theoretical prediction Eq.(8) for $\lambda = 2.74$; dotted line - experimental regression line from Resio et al. (2004a); Resio and Long (2007). Diamonds - results of numerical calculations for duration limited case with wind speed $u_{10} = 10$ m/sec.

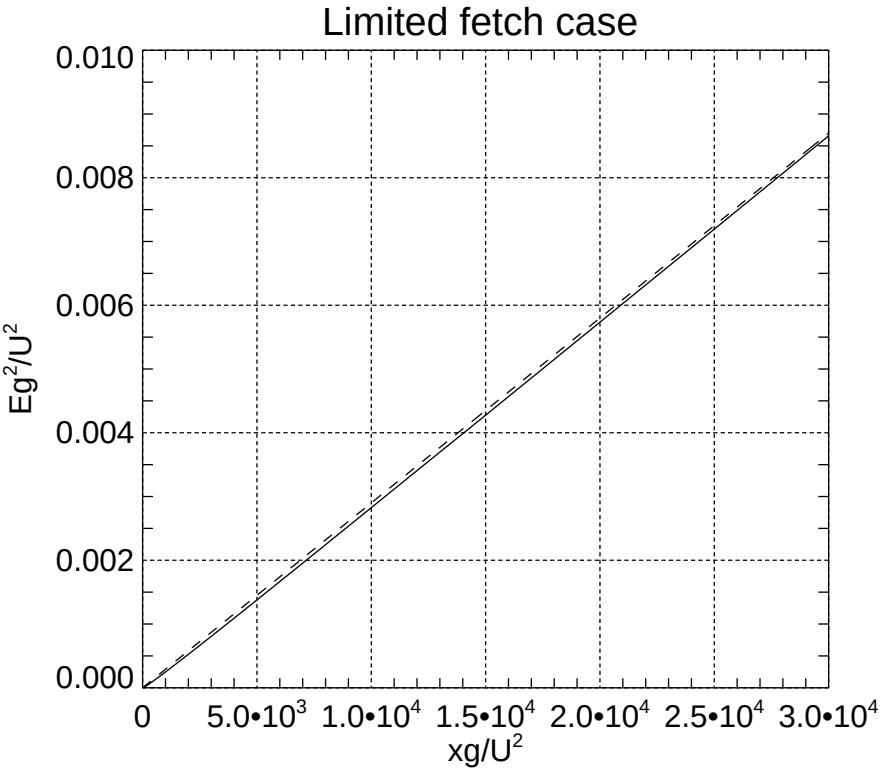

Figure 12. Dimensionless energy Eg^2/U^4 versus dimensionless fetch xg/U^2 for fetch limited case. Dashed fit $2.9 \cdot 10^{-7} xg/U^2$

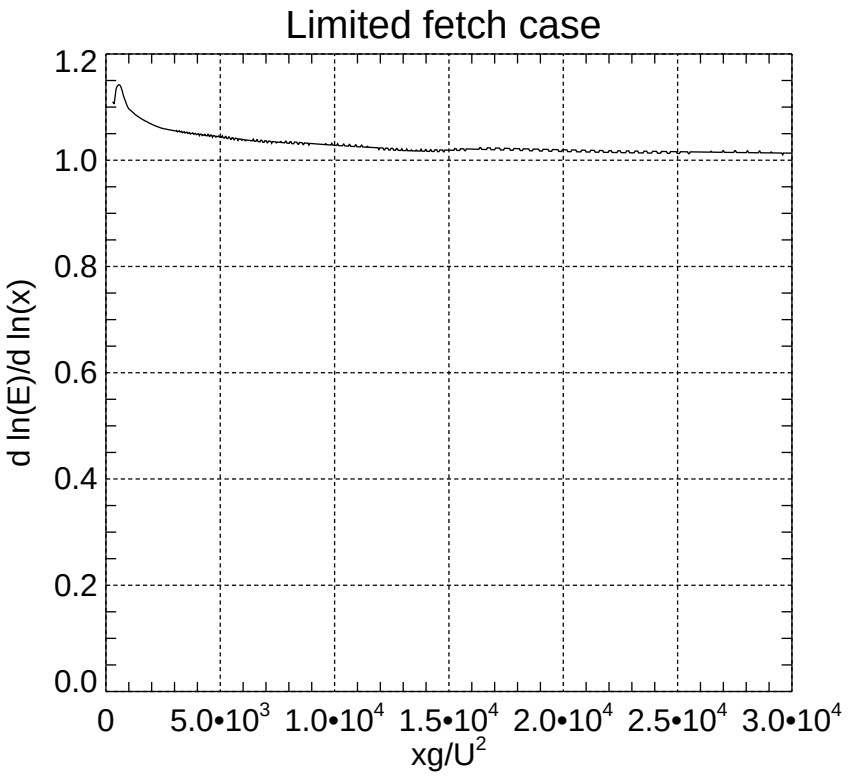

Figure 13. Local energy exponent power $p = \frac{d \ln E}{d \ln x}$ as a function of dimensionless fetch xg/U^2 for fetch limited case.

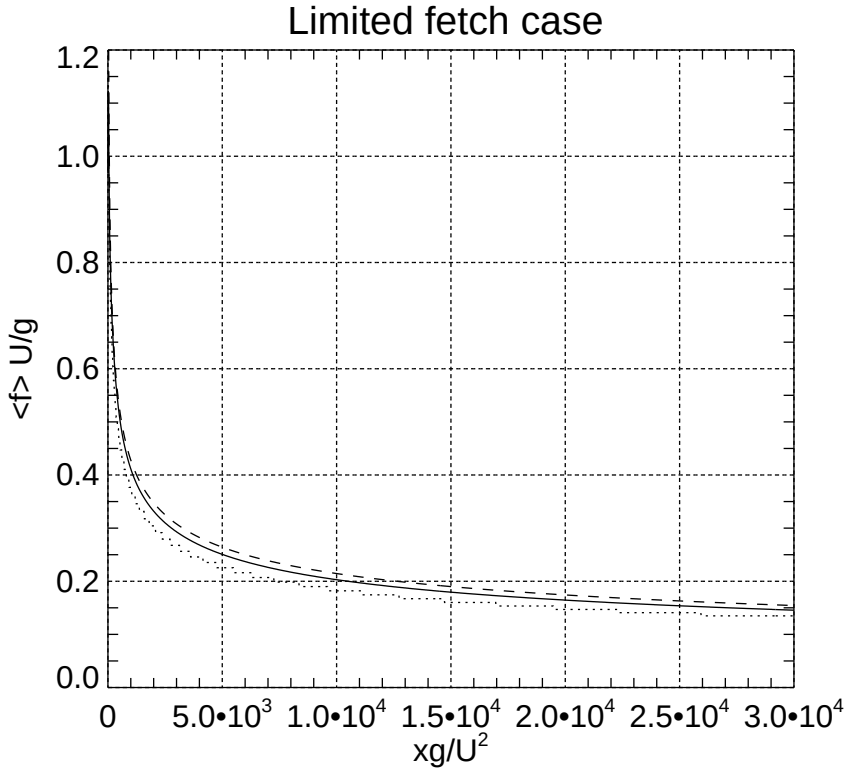

Figure 14. Dimensionless mean frequency, as a function of dimensionless fetch (solid line), calculated as $< f >= \frac{1}{2\pi}\frac{\int \omega n d\omega d\theta}{\int n d\omega d\theta}$, where $n(\omega,\theta) = \frac{\varepsilon(\omega,\theta)}{\omega}$ is the wave action spectrum. The dotted line is the peak frequency $f_p = \frac{\omega_p}{2\pi}$, and the dashed is the theoretical fit $3.4 \cdot \left(\frac{xg}{U^2}\right)^{-0.3}$.

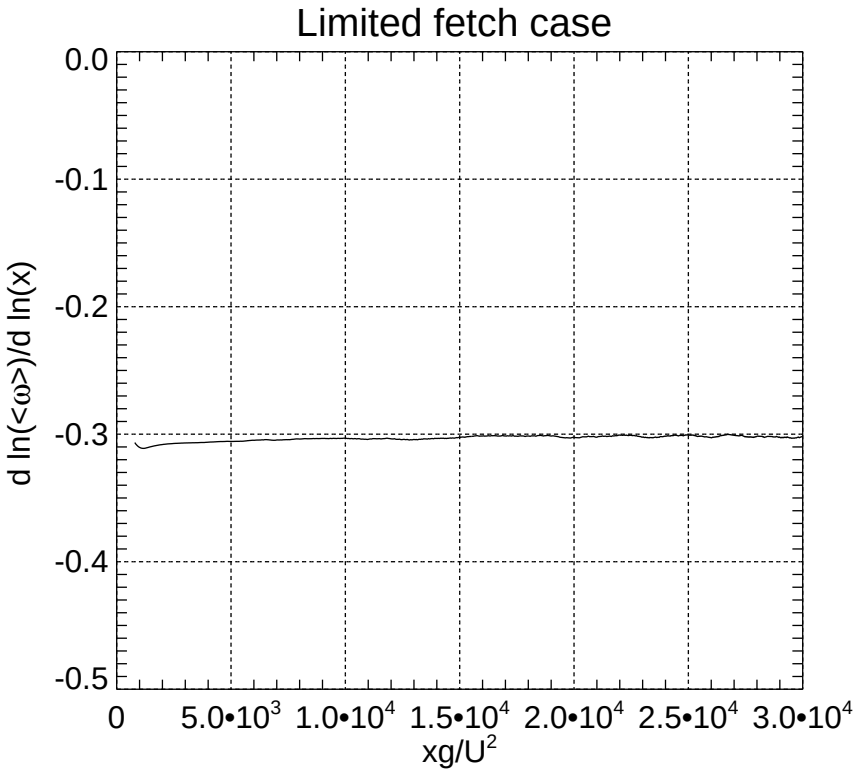

Figure 15. Local mean frequency exponent power $q = \frac{d\ln<\omega>}{d\ln x}$ as a function of dimensionless fetch xg/U^2 for fetch limited case.

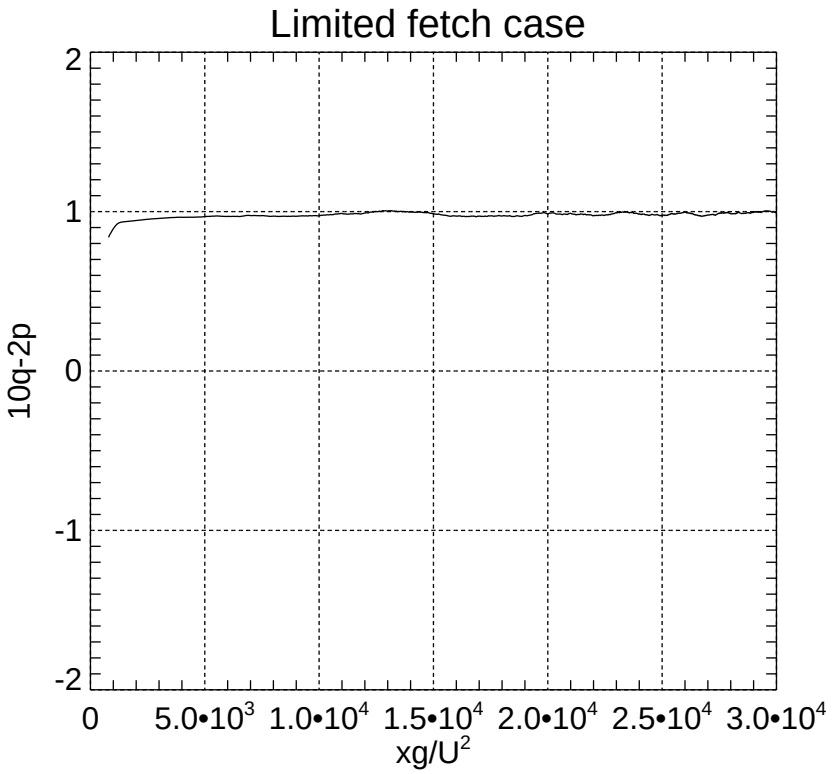

Figure 16. "Magic number" $10q - 2p$ as a function of dimensionless fetch xg/U^2 for fetch limited case.

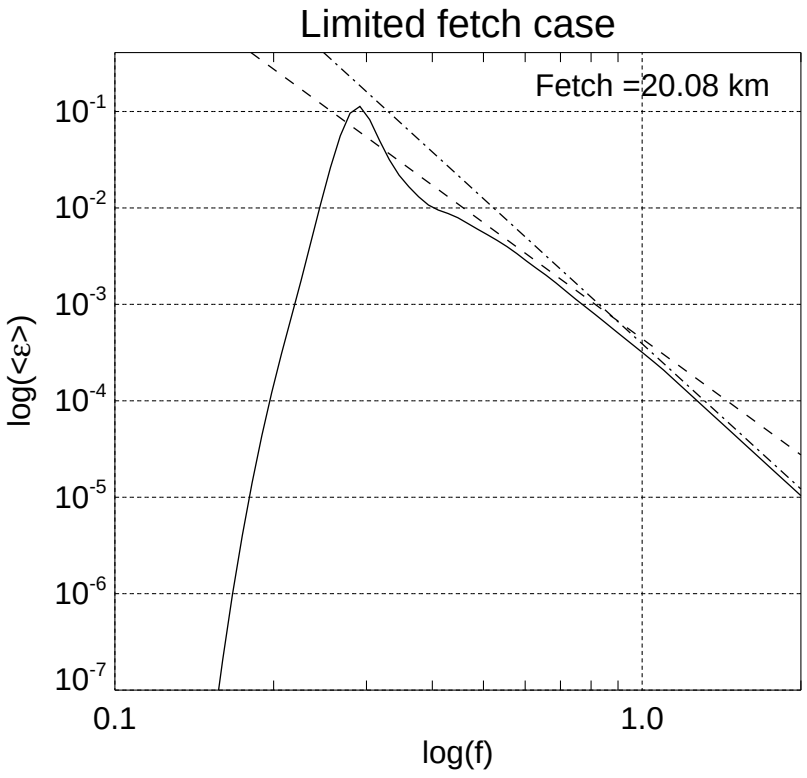

Figure 17. Decimal logarithm of the angle averaged spectrum as a function of the decimal logarithm of the frequency for fetch limited case.

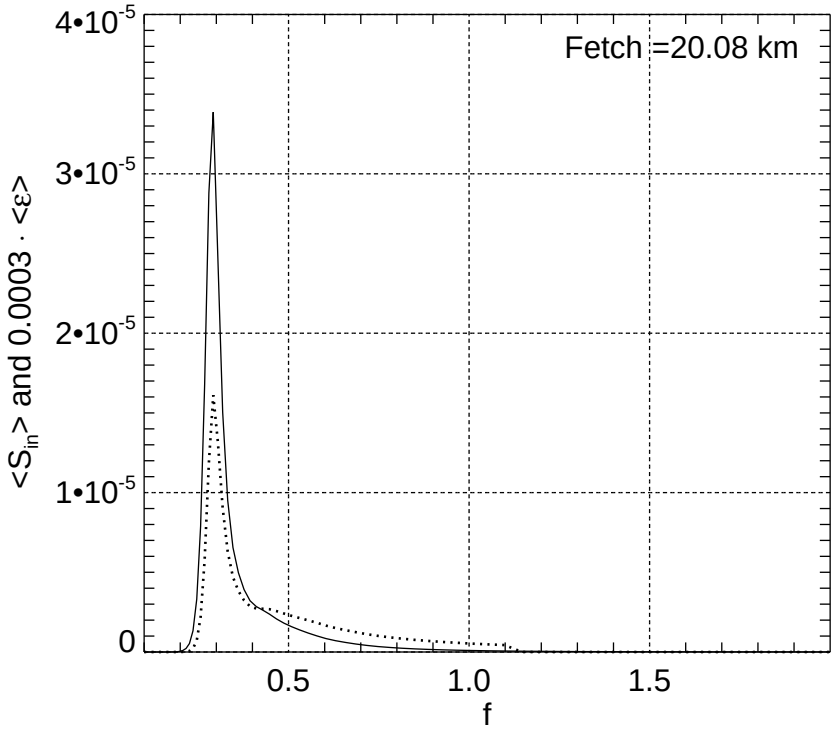

Figure 18. Typical, angle averaged, wind input function density $< S_{in} >= \frac{1}{2\pi} \int \gamma(\omega,\theta)\varepsilon(\omega,\theta)d\theta$ and angle averaged spectrum $< \varepsilon >= \frac{1}{2\pi} \int \varepsilon(\omega,\theta)d\theta$ (solid line) as the functions of the frequency $f = \frac{\omega}{2\pi}$.

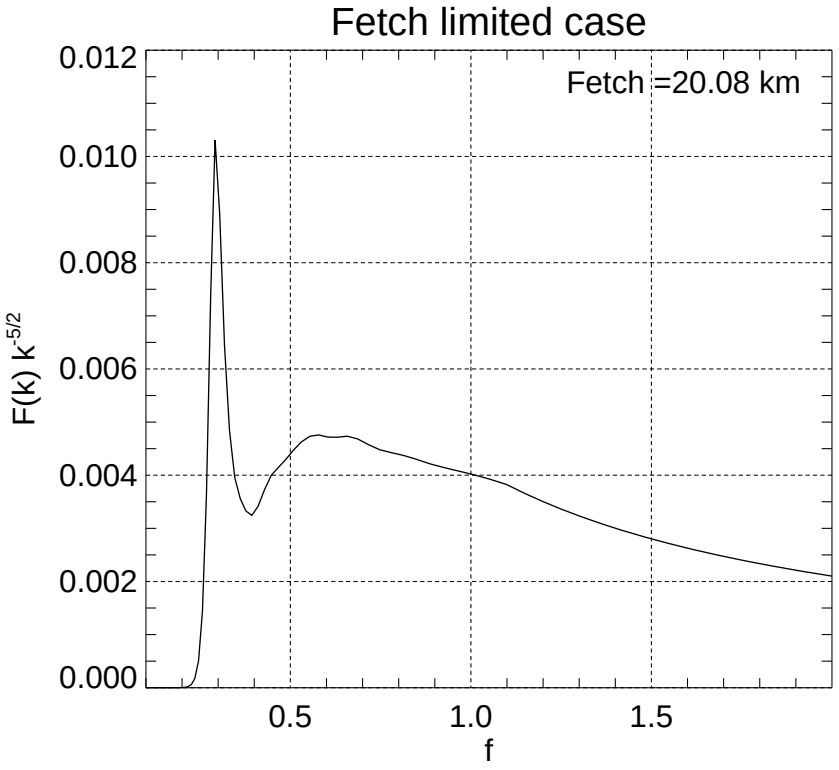

Figure 19. Compensated spectrum for fetch limited case as function of linear frequency f.

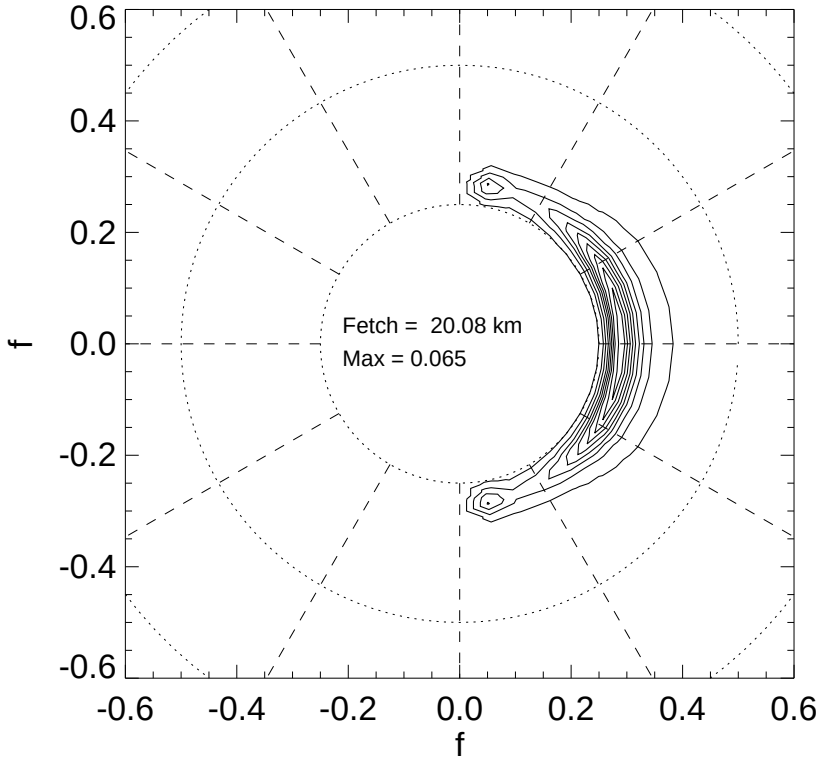

Figure 20. Angular spectra for fetch limited case.

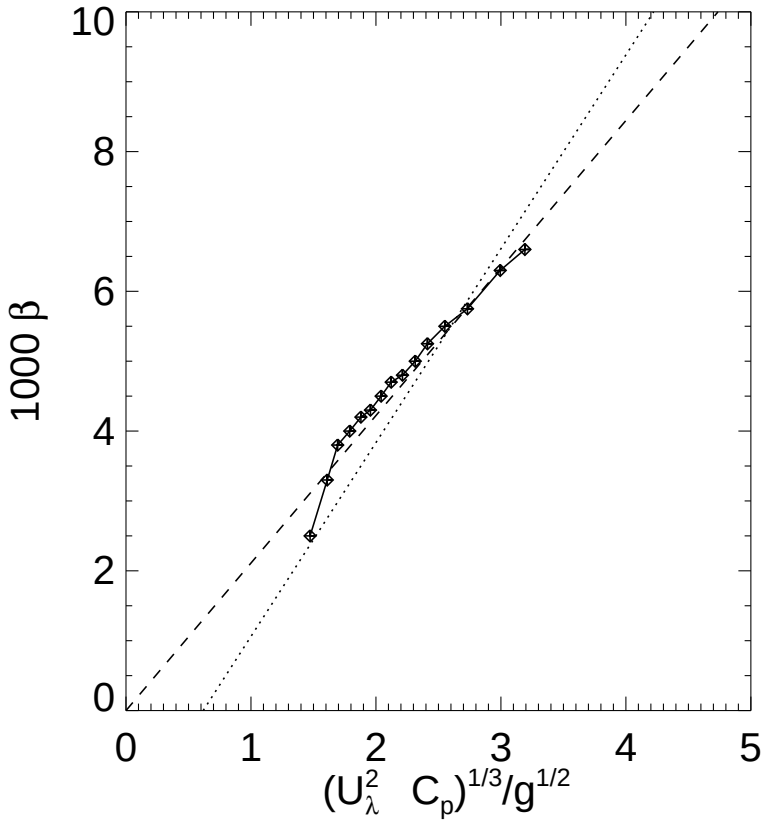

Figure 21. Experimental and numerical evidence of dependence of 1000β on $\left(u_\lambda^2 c_p\right)^{1/3}/g^{1/2}$. Dashed line - theoretical prediction Eq.(8) for $\lambda = 2.11$; dotted line - experimental regression line from Resio et al. (2004a); Resio and Long (2007). Crosses - results of numerical calculations for fetch limited case with wind speed $U = 10$ m/sec.

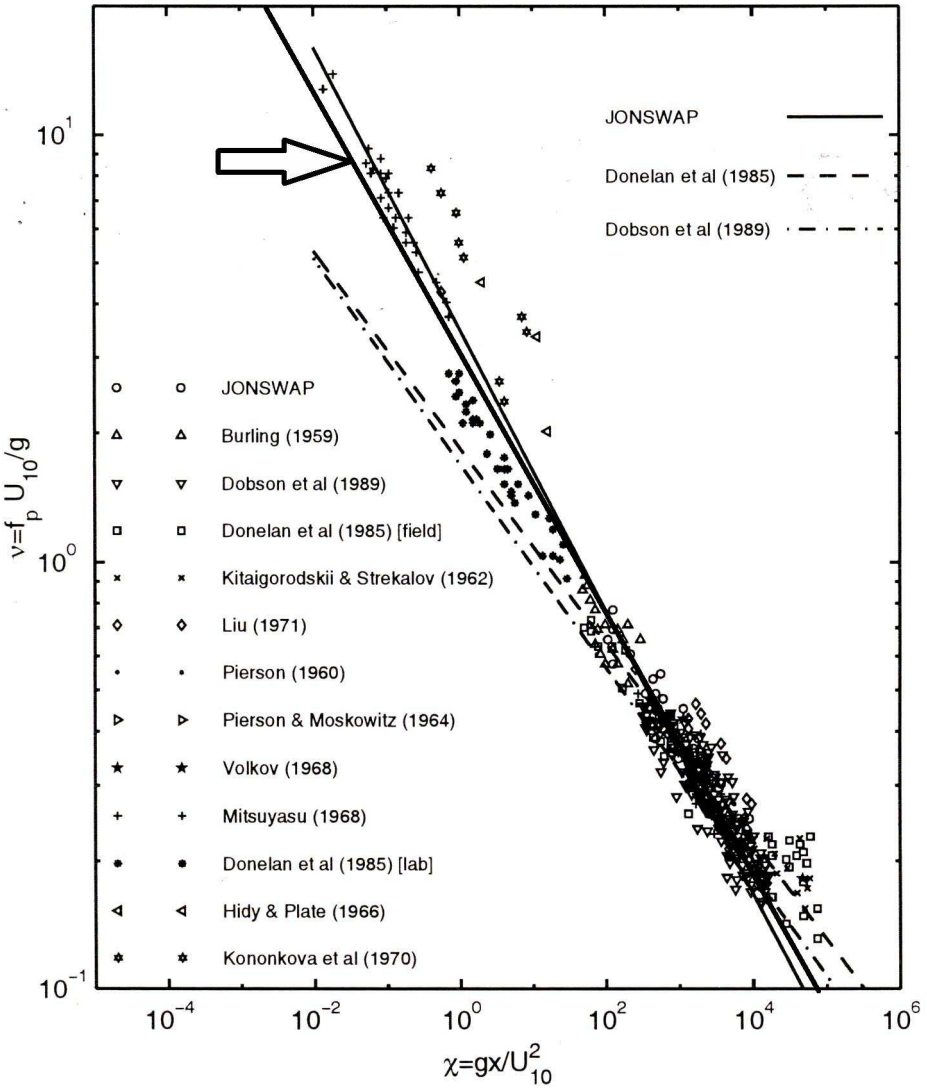

Figure 22. Solid line (pointed by arrow), presents nondimentional energy ε from the limited fetch numerical experiments, superimposed on the Figure 5.4, which is adapted from Young (1999). The original caption is: "A composite of data from variety of studies showing the development of the non-dimensional energy, ε as a function of non-dimensional fetch, χ. The original JONSWAP study (Hasselmann et al, 1973) used the data marked, JONSWAP, together with that of Burling (1959) and Mitsuyasu (1968). Also shown are a number of growth curves obtained from the various data sets. These include: JONSWAP Eq.(5.27), Donelan et al (1985) Eq,(5.33) and Dobson et al (1989) Eq.(5.38)."

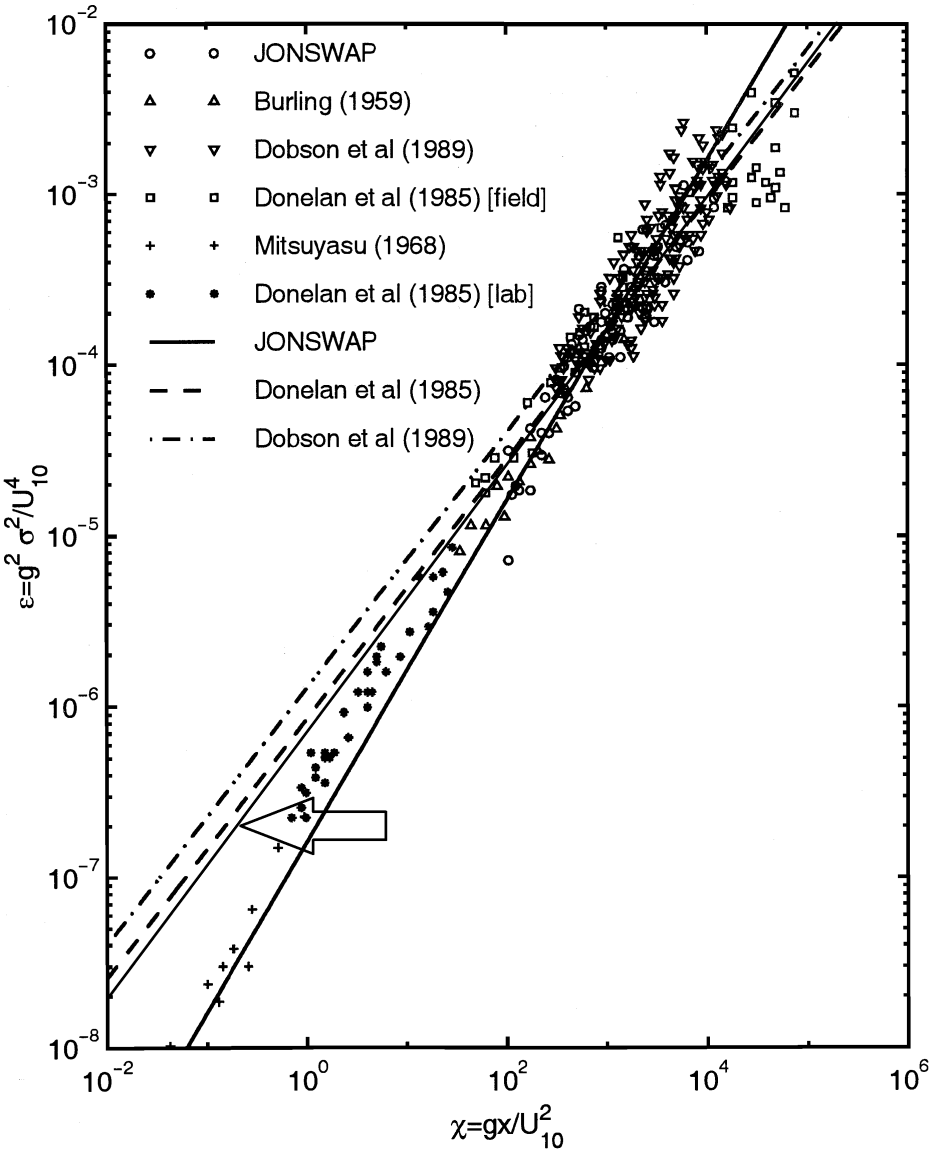

Figure 23. Solid line (pointed by arrow), presents non-dimensional frequency as the function of the fetch for limited fetch numerical experiments, superimposed on the Figure 5.5, adapted from Young (1999). The original caption is: "A composite of data from a variety of studies showing the development of the non-dimensional peak frequency, ν as a function of non-dimensional fetch, χ. The original JONSWAP study (Hasselmann et al, 1973) used all the data shown with the exception of that marked Donelan et al (1985) and Dobson et al (1989). Also shown are a number of growth curves obtained from the various data sets. These include: JONSWAP Eq.(5.28), Donelan et al (1985) Eq.(5.34) and Dobson et al (1989) Eq.(5.39)."